Northumbria
University
NEWCASTLE

Geophysical Research Letters

RESEARCH LETTER
10.1029/2019GL084365

Drying in the Middle East During Northern Hemisphere Cold Events of the Early Glacial Period

S. A. Carolin[1,2], V. Ersek[3], W. H. G. Roberts[3], R. T. Walker[1], and G. M. Henderson[1]

[1]Department of Earth Sciences, University of Oxford, Oxford, UK, [2]Now at Institute of Geology, University of Innsbruck, Innsbruck, Austria, [3]Department of Geography and Environmental Sciences, Northumbria University, Newcastle-upon-Tyne, UK

Key Points:
- Trace-element data in a northeastern Iran stalagmite suggest anomalously dry local conditions during Greenland stadial events 22–20
- Climate model results and changing Iranian oxygen-isotope gradients show evidence of a drier Middle East during these stadials

Supporting Information:
- Supporting Information S1
- Data Set S1

Correspondence to:
S. A. Carolin,
stacyanne.carolin@oeaw.ac.at

Citation:
Carolin, S. A., Ersek, V., Roberts, W. H. G., Walker, R. T., & Henderson, G. M. (2019). Drying in the Middle East during Northern Hemisphere cold events of the early glacial period. *Geophysical Research Letters*, *46*, 14,003–14,010. https://doi.org/10.1029/2019GL084365

Received 1 JUL 2019
Accepted 16 NOV 2019
Accepted article online 19 NOV 2019
Published online 4 DEC 2019

Abstract Few paleoclimate records exist to assess the central Middle East's response to natural forcing beyond the instrumental record. Here, we present a multiproxy stalagmite-based climate reconstruction from Iran's semiarid northeast that spans 100–70,000 years before present. During severe cold (stadial) events in the North Atlantic at ≈88, 77, and 73 ka, stalagmite trace-element data indicate anomalously dry periods at this location. Stadial event increases in the stalagmite oxygen isotopes mirror those in a published Iranian stalagmite 800 km to the west. A global climate model simulates drying across the Middle East region in response to stadial event forcing, in agreement with oxygen isotope enrichments in both Iranian records, caused by a smaller fractional loss of moisture on the trajectory upstream. The paleoproxies and model experiments are consistent in indicating a drier Middle East climate during the cold North Atlantic stadials.

Plain Language Summary Iran is particularly vulnerable to the effects of climate change due to its scarce water availability. Iran's climate likely changed in the past due to natural causes, indications of which can be found in climate archives such as tens-of-thousands-of-year-old cave stalagmites. Stalagmites record evidence of changes in rainfall pattern and amount. This study presents a reconstruction of both regional and local rainfall changes based on the geochemistry of stalagmites from northwest and northeast Iran. The record covers 100–70,000 years before present, a period when ice sheets covered North America and northern Europe, and Earth was experiencing multiple abrupt shifts to even colder conditions in the Northern Hemisphere. Each event's shift to colder temperatures lasted for a few thousand years. We show that both the stalagmite geochemical data and state-of-the-climate models are consistent in indicating a drier Middle East climate during these cold events.

1. Introduction

Society and ecosystems in the center of the Middle East region (Syria, Iraq, and Iran) are highly vulnerable to changes in water availability, with annual precipitation generally low, around 100–200 mm/year, outside of the higher elevation mountainous areas (European Centre for Medium-range Weather Forecast (ECMWF), 2011). Interest in investigating past climate change in this region stems from the desire to better constrain our knowledge of the system's precipitation variability and its response to various external forcings (Aubert et al., 2017; Carolin et al., 2019; Flohr et al., 2017; Mehterian et al., 2017; Sharifi et al., 2015; Sharifi et al., 2018).

Millennial stadial events of the last glacial period (110–20 ka, thousand years before 1950 CE) are useful paleoclimate episodes with which to study the Middle East region's response to a known abrupt and relatively short-lived global-scale forcing. Stadial events are characterized by a rapid expansion of North Atlantic sea ice (Dokken et al., 2013; Petersen et al., 2013) and by extension of low temperatures equatorward (Chiang & Bitz, 2005). They are associated with weakening of the Atlantic Meridional Overturning Circulation (Henry et al., 2016) and result in warming in the southern hemisphere (EPICA community members, 2006). The resulting change in the temperature gradient between the hemispheres prompts a southward shift of the intertropical convergence zone (ITCZ) during peak stadial events and a weakened Indian summer monsoon (Deplazes et al., 2013).

A handful of paleoclimate records to the west of and within the Anti-Taurus–Zagros Mountain range have reported a drier climate during stadial events in the Middle East region. These include lake and speleothem

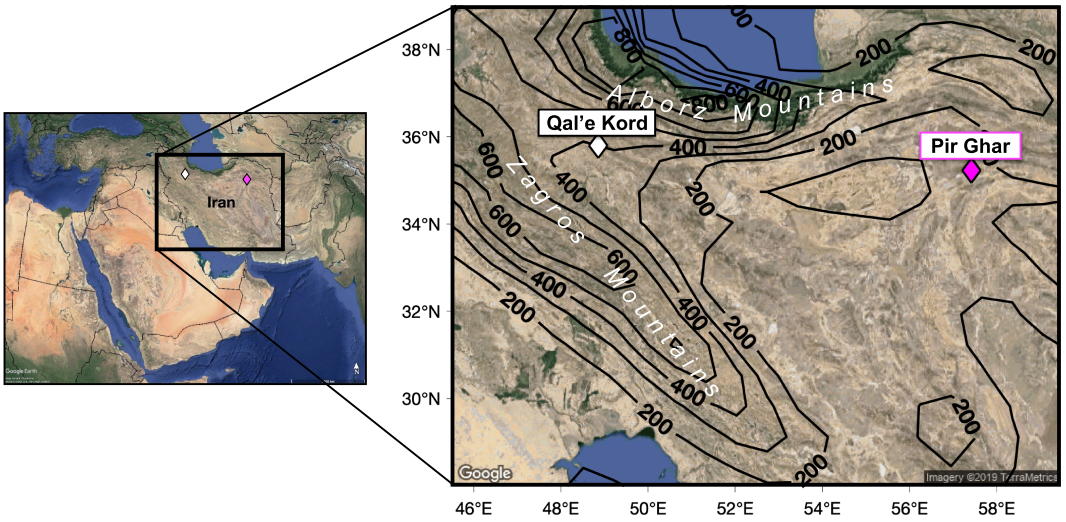

Figure 1. Iranian cave site locations. Background Google Earth image shows modern dry environment, excluding the wetter region north of the Alborz mountains. Isopleths show forecast annual precipitation, 1979–2018 (ECMWF, 2011). Qal'e Kord (white diamond, Mehterian et al., 2017) and Pir Ghar (magenta diamond, this study) cave sites are indicated. Map Imagery: ©2019 TerraMetrics.

records from northeast (NE) Turkey (Rowe et al., 2012; Stockhecke et al., 2016), stalagmite records from northwest (NW) Iran (Mehterian et al., 2017), and Arabian Sea marine eolian dust activity records (Pourmand et al., 2004; Schulz et al., 1998). Some of these studies have suggested drier conditions specifically in the winter (Mehterian et al., 2017; Rowe et al., 2012), others, drier conditions in the summer (Pourmand et al., 2004; Schulz et al., 1998) or a possible proportional increase in late spring/early summer seasonal rainfall on a smaller regional scale (Rowe et al., 2012).

No climate records far east of the Zagros Mountains range (Figure 1) have been published to test the eastward extent of the suggested dry climate of stadial events in the Middle East. In addition to extending climate information spatially, a more eastern record would also improve interpretation of regional changes in past rainfall $\delta^{18}O$. Here, we present such a record, one that includes multiple stalagmite proxies spanning 100–70 ka. The record is from Pir Ghar cave in NE Iran, the first Iranian glacial record from a stalagmite outside of the Zagros Mountains region. It is an ideal complement to existing Middle East records, particularly an existing high-resolution stalagmite $\delta^{18}O$ record from NW Iran which spans 127–73 ka (Mehterian et al., 2017) (Figure 1). The new record shows distinct increases in Mg/Ca, Sr/Ca, Ba/Ca, and $\delta^{13}C$ at ~88, 77, and 73 ka, coincident with Greenland stadial (GS) events 22–20. The record also displays $\delta^{18}O$ increases coincident with GS events 23–20, which mirror the $\delta^{18}O$ signals shown in the upstream NW Iran stalagmite record. We use a fully coupled climate model to investigate the NW and NE Iran climate response to North Atlantic stadial events suggested by the combined proxy records.

2. Cave Location, Modern Climate, and Modern Rainwater Isotopes

Pir Ghar cave is located in the NE of the Iranian plateau at 1,600 masl (35.23°N, 57.42°E) (Supporting Information Text S1) (Figure 1). Today, the area receives ~175 mm average annual precipitation, of which ~80 mm falls in the winter months and ~65 mm in March and April (ECMWF, 2011). Only ~4% of precipitation falls between June and October (ECMWF, 2011). Average surface temperatures in the area vary seasonally, between ≈33 °C in the summer and ≈3 °C in the winter.

The nearest International Atomic Energy Agency (IAEA) Global Network of Isotopes in Precipitation (GNIP) rainwater isotope monitoring station is located in Tehran (~1,200 masl), ~550 km to the west (IAEA/WMO, 2019). The Tehran GNIP site shares a similar seasonal climate with the Pir Ghar cave site (Figure S1) and is dominated by November–April rainfall. The Tehran GNIP site has 10 consecutive years of precipitation $\delta^{18}O$ data, from 1962–1972, at which time average annual amount-weighted $\delta^{18}O$ was

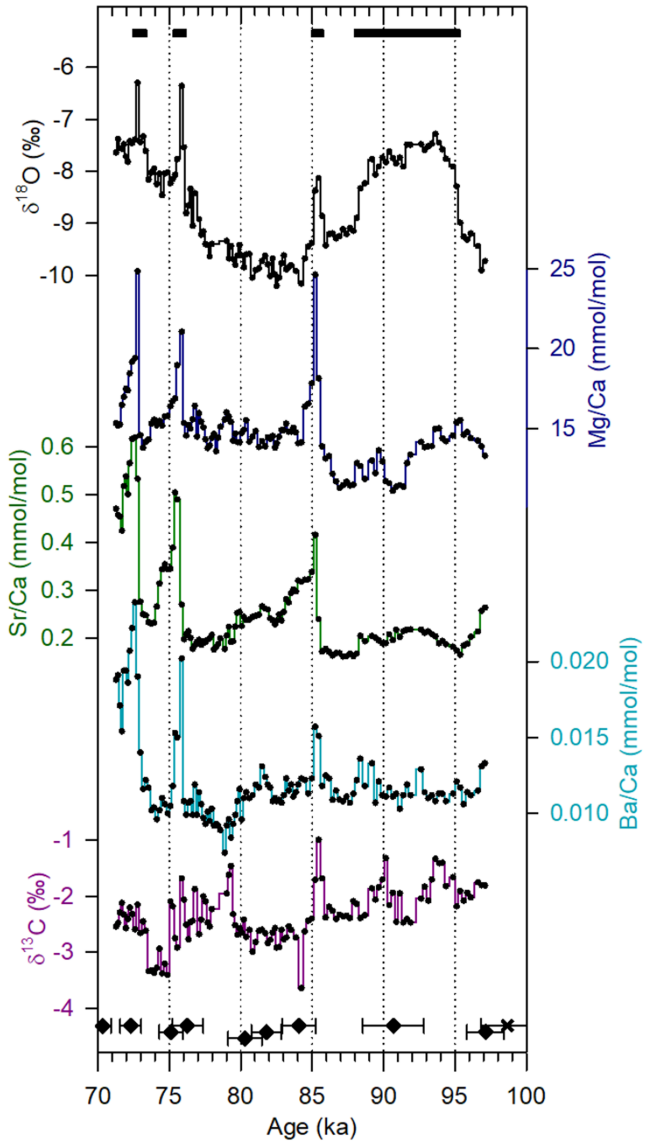

Figure 2. NE Iran stalagmite $\delta^{18}O$, $\delta^{13}C$, and element-to-calcium records. U/Th ages (black diamonds) and the hiatus boundary ("x" mark, ~99 ka) with 95% confidence ranges shown at the bottom of the figure. Black horizontal bars at the top of the figure summarize timing of increased $\delta^{18}O$ values.

$-5.4 \pm 2.4(1\sigma)$‰. A negative correlation exists between mean annual precipitation-weighted $\delta^{18}O$ and mean annual precipitation amount, in which 51% of the variance is explained (IAEA/WMO, 2019; Carolin et al., 2019 SI Appendix).

3. Stalagmite Record Construction

Pir Ghar cave stalagmite sample PG11-3 was U/Th dated in the Department of Earth Sciences at Oxford University (Text S2). An age model with associated 95% confidence ranges was constructed from 10 individual ages using OxCal (Bronk Ramsey, 2008, 2009; Bronk Ramsey & Lee, 2013) (Text S3). A boundary at one visual growth hiatus ("x" mark at the bottom of Figure 2) was specified in the OxCal model input (Text S3). The upper section of the stalagmite was found to grow at a relatively slow and constant growth rate between 100 and 70 ka (Figure S5). Stable oxygen and carbon isotopes and trace-metal-to-calcium (X/Ca) ratios were measured at 600 μm, ~200 year, resolution along the stalagmite growth axis (Text S4).

4. Stable Isotope and X/Ca Results

The PG11-3 $\delta^{18}O$ record shows a general long-term increase from ≈−10‰ at 100 ka to ≈−7.5‰ at 70 ka (Figure 2). Superimposed on this trend are four distinct periods of increased $\delta^{18}O$ values. These periods begin at 95.4 ± 1.8 ka, 85.9 ± 1.8 ka, 76.2 ± 1.1 ka, and 73.5 ± 1.1 ka, with the earliest lasting for ≈7 Kyr, and the others each lasting for ≈1 Kyr (Figure 2). All age uncertainties are listed as two standard deviations (2σ). Three of the four periods of increased $\delta^{18}O$, the shorter period events, correspond with increases in Mg/Ca, Sr/Ca, Ba/Ca, and $\delta^{13}C$ ratios (Figure 2).

5. Impact of Early Glacial Stadial Events on Iranian Climate

The periods of increased $\delta^{18}O$, $\delta^{13}C$, and X/Ca ratios in PG11-3 are coincident within error of stadial events of the early glacial period (NGRIP Members, 2004; Moseley et al., 2019) (Figure 3). Both the NW Iran (Mehterian et al., 2017) and NE Iran (this study) (Figure 1) stalagmite $\delta^{18}O$ records increase multiple permils above background levels during the stadial events (Figure 3b). Proxies which record rainfall's source water (eastern Mediterranean, Red Sea, Arabian Sea) $\delta^{18}O$ variability do not show stadial event signals during this period (Grant et al., 2012; Siddall et al., 2003; Clemens et al., 1996, respectively), and therefore, source water isotope changes are unlikely to be the origin of the Iranian stalagmites' $\delta^{18}O$ increases. Based on our interpretation of the speleothem proxies, as detailed below, we conclude that anomalous dry conditions resulted across the central Middle East due to the stadial forcing. Our interpretations are supported by models that quantify chemical evolution of karst dripwaters in responses to local environmental changes, as well as global climate model experiments that show the expected moisture transport (column integral of wind multiplied by the specific humidity) and precipitation amount changes in the region that may result from similar-type North Atlantic event forcing.

X/Ca ratios and $\delta^{13}C$ values in stalagmites can be controlled by a number of processes, such as changes in vegetation, biological activity in the soil, karst aquifer water flow rates and flow paths, temperature, and the leaching of aerosols deposited in the soil zone (e.g., Carolin et al., 2019; Day & Henderson, 2013; Dorale et al., 1992; Fairchild et al., 2000; Genty et al., 2003; Tremaine & Froelich, 2013). In general, however, there is a tendency for X/Ca and $\delta^{13}C$ to increase when there is less water flow in the rocks overlying the cave. In particular, when water flow rates are slower during drier periods, prior calcite precipitation (PCP)

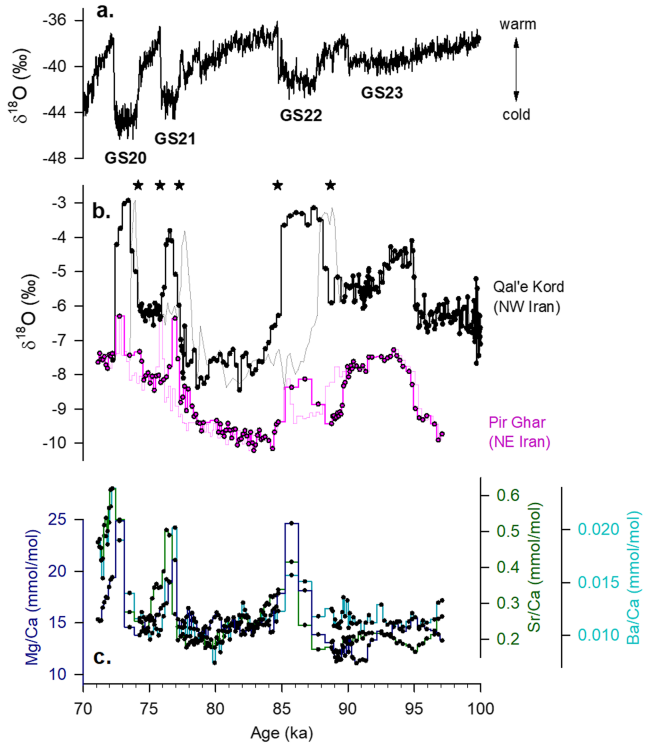

Figure 3. Comparison of the Iranian records' climate response to GS events from 100–70 ka. (a) North Greenland Ice core Project (NGRIP) $\delta^{18}O$ record, a proxy for local temperatures (lower $\delta^{18}O$ indicates colder temperatures) (NGRIP Members, 2004). Tie points (stars) at the onset and ending of GS events 22–20 (Moseley et al., 2019) were used to adjust the Greenland ice core age models. (b) NW and NE Iran speleothem $\delta^{18}O$ records (Mehterian et al., 2017; this study), plotted on their original age models using thin lines, and the adjusted age model using thick lines (Text S3). Note the NW Iran $\delta^{18}O$ values are higher than the NE Iran $\delta^{18}O$ values throughout the record. (c) Overlapping Pir Ghar (NE Iran, this study) stalagmite X/Ca ratios, plotted on the adjusted age model as in b (Text S3).

occurs to a greater extent, further increasing dripwater X/Ca ratios and $\delta^{13}C$ values as the waters travel away from the karst surface (e.g., Fairchild et al., 2000; Johnson et al., 2006; Sinclair et al., 2012).

The evolution of X/Ca ratios and $\delta^{13}C$ values in the Pir Ghar record is consistent with an increase in PCP (Figure 4), and support the interpretation of local drying during stadial events GS 22–20 at century-scale resolution. Ratios increase during the onset of the events and decrease again as the events end (Figure 4). Based on the total movement of the X/Ca values along the PCP trajectory within each event (Figure 4), we hypothesize that PCP increased to a similar extent over each event. Additionally, within the stadial events, the Mg/Ca v. Sr/Ca v. Ba/Ca v. $\delta^{13}C$ relationships change—the PCP trajectory into an event does not overlie the same PCP trajectory out of an event—indicating that the initial ratios in the karst dripwater changed during the event (Figure 4). This may have been caused by a change in dissolved bedrock mixing, possibly due to changes in soil and karst water residence time as a result of seasonal climate changes, or input of an additional endmember source, possibly eolian dust, during the event.

Oxygen isotope variations are more difficult to assess than the trace element and carbon isotopes in the Pir Ghar stalagmite, as the sample site is continental and located far from the original vapor source. The similarity between the NW (Mehterian et al., 2017) and NE (this study) Iran stalagmite records, however, is reassuring and suggests that a process is forcing rainwater isotope changes on a large scale (Figure 3b) (Cheng et al., 2013; Feng et al., 2014; Hu et al., 2008; McDermott et al., 2011; Wang et al., 2017). We posit that increases in $\delta^{18}O$ during stadials at both Iranian sites were caused by a decrease in the fraction of water vapor removal during transport along the trajectory, thus overall drier conditions upstream of both sites during stadials (e.g. Gat, 1996; Winnick et al., 2014). This interpretation is consistent with the modern GNIP data in Tehran, in which less annual precipitation is correlated with increased $\delta^{18}O$ in precipitation, though a modern interannual relationship in the data does not fully capture the processes influencing a longer timescale relationship within a different climate state and thus is noted with caution. Other controls on stalagmite $\delta^{18}O$ are not likely to be significant: First, kinetic fractionation is unlikely given the lack of correlation between $\delta^{13}C$ and $\delta^{18}O$ in PG11-3 ($r^2 = 0.05$, $p = 0.006$) and the replication of $\delta^{18}O$ signals in two locations with distinct, dissimilar environmental surroundings. Second, cooler stadial conditions would decrease evaporation on site, not increase it as required to explain an increased $\delta^{18}O$ signal by evaporation. Third, the $\delta^{18}O$ changes are too large to be attributed completely to temperature changes (Text S6). Changes in the sources of water vapor, or in its transport from these sources, are therefore the most likely to have controlled Iranian stalagmite $\delta^{18}O$ during stadial events.

We use the fully coupled climate model HadCM3 (Gordon et al., 2000; Pope et al., 2000; Valdes et al., 2017) to assess theoretical moisture transport and precipitation changes in the region in response to stadial event forcing. HadCM3 displays similar skill to CMIP5 class models in simulating spectrum climate variables (Valdes et al., 2017) and shows good qualitative agreement with the observed atmospheric flow in this region (Adler et al., 2003)(Figures S7 and S8). We note that in both the model and observations, the moisture trajectory connects the two Iranian stalagmite sites, with moisture flow crossing from NW to NE Iran (in the mean annual average and during the fall-winter-spring months when the sites receive most of their total annual precipitation) (Figures S7 and S8).

We set Last Glacial Maximum initial model state conditions (atmospheric CO_2 concentration, ice sheet extent, and orbital configuration) for the control and experiment runs. To simulate stadial events, an annual mean sea ice cover is imposed on the North Atlantic. In the stadial experiment, both the oceanic and atmospheric circulations respond to the forcing: There is a reduction in Atlantic Meridional Overturning

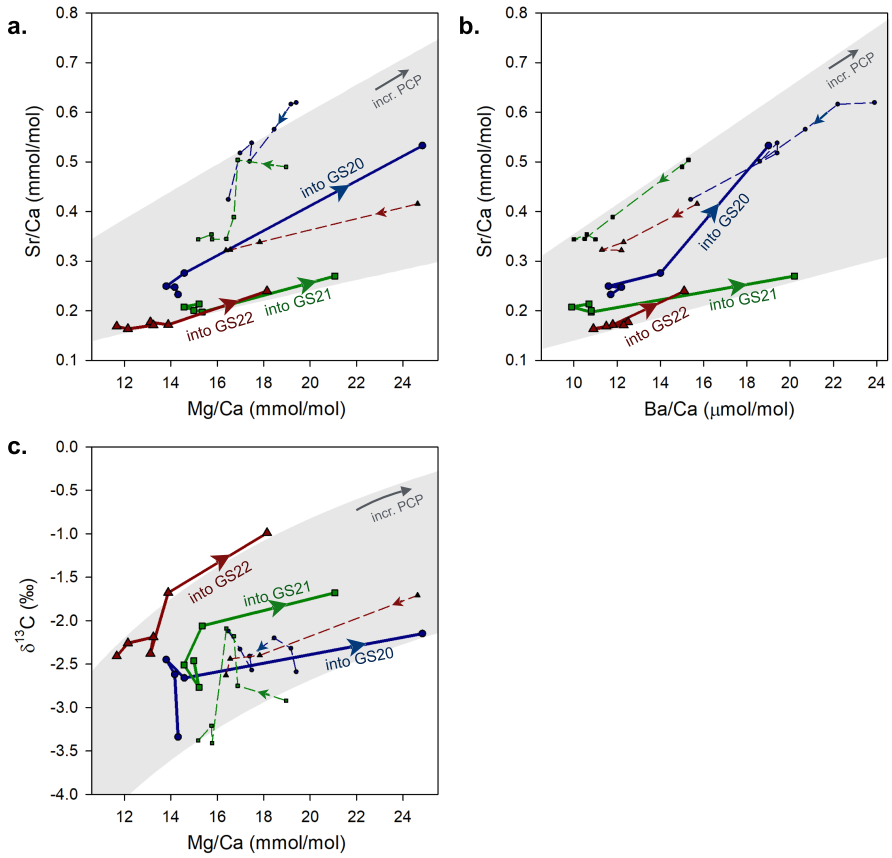

Figure 4. Crossplots suggesting an increase in prior calcite precipitation (PCP) into stadial events and a decrease out of stadial events. (a) Sr/Ca v. Mg/Ca, (b) Ba/Ca v. Sr/Ca, (c) $\delta^{13}C$ v. Mg/Ca for PG11-3 subsamples that precipitated through GS20 (blue circles), GS21 (green squares), and GS22 (red triangles). Points moving into the event are connected by a solid line, points moving out of the event are connected by a dashed line, with arrows indicating progression in time. Gray shading represents expected trajectories for PCP (Owen et al., 2018) on each figure, derived from a plausible range of initial Mg/Ca, Sr/Ca, Ba/Ca, and $\delta^{13}C$, and with partition coefficients D (*Mg*) = 0.013, D (*Sr*) = 0.12, and D (*Ba*) = 0.12 (Day & Henderson, 2013) (Text S5).

Circulation and a southern shift in the intertropical convergence zone, in agreement with global proxy records.

In the control run (glacial background state), the moisture trajectory is similar to that of modern conditions, with moisture traveling west to east across the Middle East (Figure 5a). Precipitation minus evaporation, P − E, is positive over the region during the fall-winter seasons and negative during the spring-summer seasons (Figure S9). A simple vapor transport model (Kukla et al., 2019) predicts a 2.6‰ mean annual $\delta^{18}O_{precip}$ difference between the NW and NE Iran regions using the HadCM3 control run specific humidity, relative humidity, and advection velocity parameters (using a zero topography approximation, consistent with the NE region being at lower elevation than the NW Zagros mountains (Figure S11)) (Text S7). The NW and NE Iran stalagmite $\delta^{18}O$ records are offset by ~2–3‰, with the NE site more negative, throughout the 100–70 ka record. Thus, both the stalagmite $\delta^{18}O$ proxy and the model outputs support the conclusion of moisture loss and isotope depletion along a NW to NE moisture trajectory path.

During stadial events, the HadCM3 simulation shows drying across the region (Figure 5b). In NE Iran, the modeled decrease in mean annual rainfall is ~20%. This drying is in agreement with the Pir Ghar X/Ca and $\delta^{13}C$ increases, which indicate local drying during the events (Figures 3 and 4). There is no change in the moisture trajectory during the stadial events and strong drying upstream of the NW Iran site (area between the east Mediterranean and the Zagros Mountains (Figure 5b). The model results are thus in agreement with

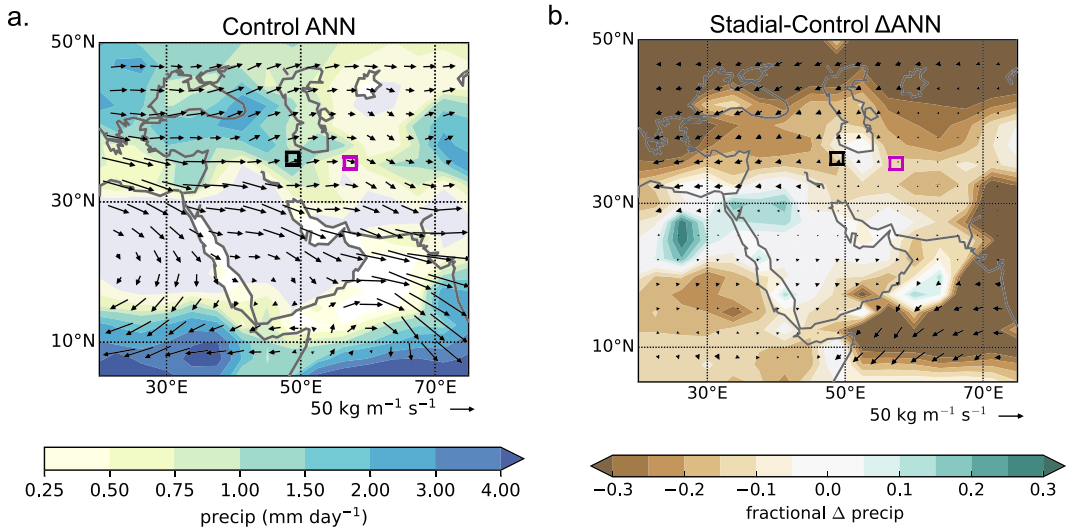

Figure 5. Modeled moisture changes in the Middle East during stadial events using LGM boundary conditions. (a) Control run mean annual precipitation and moisture transport. Contour colors show precipitation amount. Arrows indicate the moisture transport vector, calculated as the column integral of wind multiplied by specific humidity. (b) Changes in mean annual precipitation and moisture transport due to the stadial event. Contour colors show the fractional change in precipitation amount and arrows indicate the change in the moisture transport vector, stadial minus control.

the significant increases in $\delta^{18}O$ observed in both NW and NE Iran during stadial events and can be attributed to a smaller fractional loss of moisture and Rayleigh distillation upstream of the cave sites.

Comparison between the two Iranian stalagmite $\delta^{18}O$ records further reveals a greater $\delta^{18}O$ increase in NW Iran than in NE Iran during stadials (Figure 3b). The model seasonal results offer a possible explanation for this. The difference between NW and NE Iran total atmospheric column moisture, due to loss of moisture on the trajectory from west to east, is ~10% larger during stadial event winters. This results in a greater modeled $\delta^{18}O$ difference between NW and NE area precipitation $\delta^{18}O$, with the calculated precipitation-weighted mean annual difference increasing under stadial conditions from 2.6‰ to 3.0‰ (Text S7). This 0.4‰ modeled $\delta^{18}O$ offset increase is approximately similar to the ~1‰ offset increase seen in the stalagmite records during stadial events (Figure 3b). An alternative explanation to the larger $\delta^{18}O$ stadial event offset is a change in the fraction of moisture from different moisture sources at either site, possibly including the relatively depleted Caspian Sea source, during stadial events.

Finally, we note that unlike GS events 22–20, local drying in NE Iran is not evident in the stalagmite trace-element records during GS23 (Figure 3c), although our record and the NW record do show ~2‰ increases in $\delta^{18}O$ (Figure 3b). We propose that the regional climate response to this event differed from that to GS events 22–20, thus creating a $\delta^{18}O$ signal but no local precipitation change in NE Iran. Of the four events within 100–70 ka, Greenland ice core $\delta^{18}O$ changes least during the relatively long duration GS23 (NGRIP Members, 2004) (Figure 3a). Chinese stalagmite $\delta^{18}O$ values also do not show any abrupt change associated with GS23, indicating that the Asian monsoon system likely did not respond to any millennial scale forcings during this event (Cheng et al., 2016), further differentiating it from the other stadial in the 100–70 ka period.

6. Conclusions

The 100–70 ka NE Iran stalagmite record presented in this study assists in identifying the Middle East region's response to a North Atlantic-forced climate perturbation. Mg/Ca, Sr/Ca, Ba/Ca, and $\delta^{13}C$ in the stalagmite show clear increases during GS events 22–20. Correlations between the ratios support the interpretation of a common forcing—increased PCP in the karst aquifer—which points to local drying occurring during these events. Significant increases in stalagmite $\delta^{18}O$ are coincident with the X/Ca and $\delta^{13}C$ increases, a signal mirrored in a second Iranian stalagmite $\delta^{18}O$ record 800 km to the west. Stadial event climate experiments simulate drying across the region in response to the event forcing. The model results are in

agreement with significant $\delta^{18}O$ enrichments during stadials in NW and NE Iran caused by a smaller fractional loss of moisture and Rayleigh distillation upstream of the cave sites. Thus, the paleo-proxies and model experiments both support the conclusion that anomalously dry conditions resulted across the central Middle East during stadial periods, a significant climate response to an external forcing in this critical region.

Acknowledgments
We thank Morteza Talebian from the Geological Survey of Iran and Vahid Ashrafi, Saeed Hasheminezhad, and Javad Nezamdoost from the Iranian Cave and Speleology Association, who were instrumental in fieldwork and sample collection. We thank Chris Day for his helpful comments on proxy interpretation, Oxford undergraduate Jacob Morgan (now at Scripps Institute of Oceanography) for his assistance in milling and measuring stable isotope and trace element samples, Alan Hsieh and Phil Holdship for assistance with the MC-ICP-MS and trace element ICP-MS. This research was supported by the Leverhulme Trust, Research Project RPG-2013-235, the Royal Geographical Society Thesiger-Oman Fellowship, and the British Cave Research Association Ghar Parau Foundation Expedition Grant. Data supporting the conclusions of this paper are archived at NCDC (https://www.ncdc.noaa.gov/data-access/paleoclimatology-data/datasets/speleothem). We thank Daniel Ibarra and three anonymous reviewers for suggestions and edits that improved this manuscript.

References

Adler, R. F., Huffman, G. J., Chang, A., Ferraro, R., Xie, P.-P., Janowiak, J., et al. (2003). The version-2 global precipitation climatology project (GPCP) monthly precipitation analysis (1979–Present). *Journal of Hydrometeorology*, *4*(6), 1147–1167. https://doi.org/10.1175/1525-7541(2003)004<1147:TVGPCP>2.0.CO;2

Aubert, C., Brisset, E., Djamali, M., Sharifi, A., Ponel, P., Gambin, B., et al. (2017). Late glacial and early Holocene hydroclimate variability in northwest Iran (Talesh Mountains) inferred from chironomid and pollen analysis. *Journal of Paleolimnology*, *58*(2), 151–167. https://doi.org/10.1007/s10933-017-9969-8

Bronk Ramsey, C. (2008). Deposition models for chronological records. *Quaternary Science Reviews*, *27*(1–2), 42–60. https://doi.org/10.1016/j.quascirev.2007.01.019

Bronk Ramsey, C. (2009). Bayesian analysis of radiocarbon dates. *Radiocarbon*, *51*(01), 337–360. https://doi.org/10.1017/S0033822200033865

Bronk Ramsey, C. B., & Lee, S. (2013). Recent and planned developments of the program OxCal. *Radiocarbon*, *55*(02), 720–730. https://doi.org/10.1017/S0033822200057878

Carolin, S. A., Walker, R. T., Day, C. C., Ersek, V., Sloan, R. A., Dee, M. W., et al. (2019). Precise timing of abrupt increase in dust activity in the Middle East coincident with 4.2 ka social change. *Proceedings of the National Academy of Sciences*, *116*(1), 67–72. https://doi.org/10.1073/pnas.1808103115

Cheng, H., Edwards, R. L., Sinha, A., Spötl, C., Yi, L., Chen, S., et al. (2016). The Asian monsoon over the past 640,000 years and ice age terminations. *Nature*, *534*(7609), 640–646. https://doi.org/10.1038/nature18591

Cheng, H., Sinha, A., Cruz, F. W., Wang, X., Edwards, R. L., d'Horta, F. M., et al. (2013). Climate change patterns in Amazonia and biodiversity. *Nature Communications*, *4*(1), 1411. https://doi.org/10.1038/ncomms2415

Chiang, J. C. H., & Bitz, C. M. (2005). Influence of high latitude ice cover on the marine Intertropical Convergence Zone. *Climate Dynamics*, *25*(5), 477–496. https://doi.org/10.1007/s00382-005-0040-5

Clemens, S. C., Murray, D. W., & Prell, W. L. (1996). Nonstationary Phase of the Plio-Pleistocene Asian Monsoon. *Science*, *274*(5289), 943–948. https://doi.org/10.1126/science.274.5289.943

Day, C. C., & Henderson, G. M. (2013). Controls on trace-element partitioning in cave-analogue calcite. *Geochimica et Cosmochimica Acta*, *120*, 612–627. https://doi.org/10.1016/j.gca.2013.05.044

Deplazes, G., Lückge, A., Peterson, L. C., Timmermann, A., Hamann, Y., Hughen, K. A., et al. (2013). Links between tropical rainfall and North Atlantic climate during the last glacial period. *Nature Geoscience*, *6*(3), 213–217. https://doi.org/10.1038/ngeo1712

Dokken, T. M., Nisancioglu, K. H., Li, C., Battisti, D. S., & Kissel, C. (2013). Dansgaard-Oeschger cycles: Interactions between ocean and sea ice intrinsic to the Nordic seas: D-O cycles as seen in the nordic seas. *Paleoceanography*, *28*, 491–502. https://doi.org/10.1002/palo.20042

Dorale, J. A., Gonzalez, L. A., Reagan, M. K., Pickett, D. A., Murrell, M. T., & Baker, R. G. (1992). A high-resolution record of holocene climate change in speleothem calcite from Cold Water Cave, northeast Iowa. *Science*, *258*(5088), 1626–1630. https://doi.org/10.1126/science.258.5088.1626

EPICA Community Members (2006). One-to-one coupling of glacial climate variability in Greenland and Antarctica. *Nature*, *444*(7116), 195–198. https://doi.org/10.1038/nature05301

European Centre for Medium-range Weather Forecast (ECMWF) (2011). The ERA-Interim reanalysis dataset, Copernicus Climate Change Service (C3S) (accessed 2019), available from https://cds.climate.copernicus.eu/cdsapp#!/dataset/ecv-for-climate-change?tab=form

Fairchild, I. J., Borsato, A., Tooth, A. F., Frisia, S., Hawkesworth, C. J., Huang, Y., et al. (2000). Controls on trace element (Sr–Mg) compositions of carbonate cave waters: Implications for speleothem climatic records. *Chemical Geology*, *166*(3–4), 255–269. https://doi.org/10.1016/S0009-2541(99)00216-8

Feng, W., Hardt, B. F., Banner, J. L., Meyer, K. J., James, E. W., Musgrove, M., et al. (2014). Changing amounts and sources of moisture in the U.S. southwest since the Last Glacial Maximum in response to global climate change. *Earth and Planetary Science Letters*, *401*, 47–56. https://doi.org/10.1016/j.epsl.2014.05.046

Flohr, P., Fleitmann, D., Zorita, E., Sadekov, A., Cheng, H., Bosomworth, M., et al. (2017). Late Holocene droughts in the Fertile Crescent recorded in a speleothem from northern Iraq. *Geophysical Research Letters*, *44*, 1528–1536. https://doi.org/10.1002/2016GL071786

Gat, J. R. (1996). Oxygen and hydrogen isotopes in the hydrologic cycle. *Annual Review of Earth and Planetary Sciences*, *24*(1), 225–262. https://doi.org/10.1146/annurev.earth.24.1.225

Genty, D., Blamart, D., Ouahdi, R., Gilmour, M., Baker, A., Jouzel, J., & Van-Exter, S. (2003). Precise dating of Dansgaard–Oeschger climate oscillations in western Europe from stalagmite data. *Nature*, *421*(6925), 833–837. https://doi.org/10.1038/nature01391

Gordon, C., Cooper, C., Senior, C. A., Banks, H., Gregory, J. M., Johns, T. C., et al. (2000). The simulation of SST, sea ice extents and ocean heat transports in a version of the Hadley Centre coupled model without flux adjustments. *Climate Dynamics*, *16*(2–3), 147–168. https://doi.org/10.1007/s003820050010

Grant, K. M., Rohling, E. J., Bar-Matthews, M., Ayalon, A., Medina-Elizalde, M., Ramsey, C. B., et al. (2012). Rapid coupling between ice volume and polar temperature over the past 150,000 years. *Nature*, *491*(7426), 744–747. https://doi.org/10.1038/nature11593

Henry, L. G., McManus, J. F., Curry, W. B., Roberts, N. L., Piotrowski, A. M., & Keigwin, L. D. (2016). North Atlantic ocean circulation and abrupt climate change during the last glaciation. *Science*, *353*(6298), 470–474. https://doi.org/10.1126/science.aaf5529

Hu, C., Henderson, G. M., Huang, J., Xie, S., Sun, Y., & Johnson, K. R. (2008). Quantification of Holocene Asian monsoon rainfall from spatially separated cave records. *Earth and Planetary Science Letters*, *266*(3–4), 221–232. https://doi.org/10.1016/j.epsl.2007.10.015

International Atomic Energy Agency/World Meteorological Organization (2019). Data from "Global network of isotopes in precipitation." The GNIP Database. Available at www-naweb.iaea.org/napc/ih/IHS_resources_isohis.html.

Johnson, K., Hu, C., Belshaw, N., & Henderson, G. (2006). Seasonal trace-element and stable-isotope variations in a Chinese speleothem: The potential for high-resolution paleomonsoon reconstruction. *Earth and Planetary Science Letters*, *244*(1–2), 394–407. https://doi.org/10.1016/j.epsl.2006.01.064

Kukla, T., Winnick, M. J., Maher, K., Ibarra, D. E., & Chamberlain, C. P. (2019). The sensitivity of terrestrial δ^{18}O gradients to hydroclimate evolution. *Journal of Geophysical Research: Atmospheres*, *124*, 563–582. https://doi.org/10.1029/2018JD029571

McDermott, F., Atkinson, T. C., Fairchild, I. J., Baldini, L. M., & Mattey, D. P. (2011). A first evaluation of the spatial gradients in δ18O recorded by European Holocene speleothems. *Global and Planetary Change*, *79*(3–4), 275–287. https://doi.org/10.1016/j.gloplacha.2011.01.005

Mehterian, S., Pourmand, A., Sharifi, A., Lahijani, H. A. K., Naderi, M., & Swart, P. K. (2017). Speleothem records of glacial/interglacial climate from Iran forewarn of future Water Availability in the interior of the Middle East. *Quaternary Science Reviews*, *164*, 187–198. https://doi.org/10.1016/j.quascirev.2017.03.028

Moseley, G. E., Spötl, C., Brandstätter, S., Erhardt, T., Luetscher, M., & Edwards, R. L. (2019). NALPS19: Sub-orbital scale climate variability recorded in Northern Alpine speleothems during the last glacial period. *Climate of the Past Discussions*, 1–25. https://doi.org/10.5194/cp-2019-44

North Greenland Ice Core Project members (2004). High-resolution record of Northern Hemisphere climate extending into the last interglacial period. *Nature*, *431*(7005), 147–151. https://doi.org/10.1038/nature02805

Owen, R., Day, C. C., & Henderson, G. M. (2018). CaveCalc: A new model for speleothem chemistry & isotopes. *Computers & Geosciences*, *119*, 115–122. https://doi.org/10.1016/j.cageo.2018.06.011

Petersen, S. V., Schrag, D. P., & Clark, P. U. (2013). A new mechanism for Dansgaard-Oeschger cycles. *Paleoceanography*, *28*, 24–30. https://doi.org/10.1029/2012PA002364

Pope, V. D., Gallani, M. L., Rowntree, P. R., & Stratton, R. A. (2000). The impact of new physical parametrizations in the Hadley Centre climate model: HadAM3. *Climate Dynamics*, *16*(2–3), 123–146. https://doi.org/10.1007/s003820050009

Pourmand, A., Marcantonio, F., & Schulz, H. (2004). Variations in productivity and eolian fluxes in the northeastern Arabian Sea during the past 110 ka. *Earth and Planetary Science Letters*, *221*(1–4), 39–54. https://doi.org/10.1016/S0012-821X(04)00109-8

Rowe, P. J., Mason, J. E., Andrews, J. E., Marca, A. D., Thomas, L., van Calsteren, P., et al. (2012). Speleothem isotopic evidence of winter rainfall variability in northeast Turkey between 77 and 6 ka. *Quaternary Science Reviews*, *45*, 60–72. https://doi.org/10.1016/j.quascirev.2012.04.013

Schulz, H., von Rad, U., Erlenkeuser, H., & von Rad, U. (1998). Correlation between Arabian Sea and Greenland climate oscillations of the past 110,000 years. *Nature*, *393*(6680), 54–57. https://doi.org/10.1038/31750

Sharifi, A., Murphy, L. N., Pourmand, A., Clement, A. C., Canuel, E. A., Naderi Beni, A., et al. (2018). Early-Holocene greening of the Afro-Asian dust belt changed sources of mineral dust in West Asia. *Earth and Planetary Science Letters*, *481*, 30–40. https://doi.org/10.1016/j.epsl.2017.10.001

Sharifi, A., Pourmand, A., Canuel, E. A., Ferer-Tyler, E., Peterson, L. C., Aichner, B., et al. (2015). Abrupt climate variability since the last deglaciation based on a high-resolution, multi-proxy peat record from NW Iran: The hand that rocked the Cradle of Civilization? *Quaternary Science Reviews*, *123*, 215–230. https://doi.org/10.1016/j.quascirev.2015.07.006

Siddall, M., Rohling, E. J., Almogi-Labin, A., Hemleben, C., Meischner, D., Schmelzer, I., & Smeed, D. A. (2003). Sea-level fluctuations during the last glacial cycle. *Nature*, *423*(6942), 853–858. https://doi.org/10.1038/nature01690

Sinclair, D. J., Banner, J. L., Taylor, F. W., Partin, J., Jenson, J., Mylroie, J., et al. (2012). Magnesium and strontium systematics in tropical speleothems from the Western Pacific. *Chemical Geology*, *294-295*, 1–17. https://doi.org/10.1016/j.chemgeo.2011.10.008

Stockhecke, M., Timmermann, A., Kipfer, R., Haug, G. H., Kwiecien, O., Friedrich, T., et al. (2016). Millennial to orbital-scale variations of drought intensity in the Eastern Mediterranean. *Quaternary Science Reviews*, *133*, 77–95. https://doi.org/10.1016/j.quascirev.2015.12.016

Tremaine, D. M., & Froelich, P. N. (2013). Speleothem trace element signatures: A hydrologic geochemical study of modern cave dripwaters and farmed calcite. *Geochimica et Cosmochimica Acta*, *121*, 522–545. https://doi.org/10.1016/j.gca.2013.07.026

Valdes, P. J., Armstrong, E., Badger, M. P. S., Bradshaw, C. D., Bragg, F., Crucifix, M., et al. (2017). The BRIDGE HadCM3 family of climate models: HadCM3@Bristol v1.0. *Geoscientific Model Development*, *10*(10), 3715–3743. https://doi.org/10.5194/gmd-10-3715-2017

Wang, X., Edwards, R. L., Auler, A. S., Cheng, H., Kong, X., Wang, Y., et al. (2017). Hydroclimate changes across the Amazon lowlands over the past 45,000 years. *Nature*, *541*(7636), 204–207. https://doi.org/10.1038/nature20787

Winnick, M. J., Chamberlain, C. P., Caves, J. K., & Welker, J. M. (2014). Quantifying the isotopic 'continental effect'. *Earth and Planetary Science Letters*, *406*, 123–133. https://doi.org/10.1016/j.epsl.2014.09.005

References From the Supporting Information

Coplen, T. B. (2007). Calibration of the calcite–water oxygen-isotope geothermometer at Devils Hole, Nevada, a natural laboratory. *Geochimica et Cosmochimica Acta*, *71*(16), 3948–3957. https://doi.org/10.1016/j.gca.2007.05.028

Dietzel, M., Tang, J., Leis, A., & Köhler, S. J. (2009). Oxygen isotopic fractionation during inorganic calcite precipitation—Effects of temperature, precipitation rate and pH. *Chemical Geology*, *268*(1–2), 107–115. https://doi.org/10.1016/j.chemgeo.2009.07.015

Edwards, R. L., Chen, J. H., & Wasserburg, G. J. (1987). 238 U-234 U-230Th-232Th systematics and the precise measurement of time over the past 500,000 years. *Earth and Planetary Science Letters*, *81*(2–3), 175–192. https://doi.org/10.1016/0012-821X(87)90154-3

Hendy, C. H. (1971). The isotopic geochemistry of speleothems—I. The calculation of the effects of different modes of formation on the isotopic composition of speleothems and their applicability as palaeoclimatic indicators. *Geochimica et Cosmochimica Acta*, *35*(8), 801–824. https://doi.org/10.1016/0016-7037(71)90127-X

Horita, J., & Wesolowski, D. J. (1994). Liquid-vapor fractionation of oxygen and hydrogen isotopes of water from the freezing to the critical temperature. *Geochimica et Cosmochimica Acta*, *58*(16), 3425–3437. https://doi.org/10.1016/0016-7037(94)90096-5

Kageyama, M., Merkel, U., Otto-Bliesner, B., Prange, M., Abe-Ouchi, A., Lohmann, G., et al. (2013). Climatic impacts of fresh water hosing under Last Glacial Maximum conditions: A multi-model study. *Climate of the Past*, *9*(2), 935–953. https://doi.org/10.5194/cp-9-935-2013

Kim, S.-T., & O'Neil, J. R. (1997). Equilibrium and nonequilibrium oxygen isotope effects in synthetic carbonates. *Geochimica et Cosmochimica Acta*, *61*(16), 3461–3475. https://doi.org/10.1016/S0016-7037(97)00169-5

Ludwig, K. R., (1991). ISOPLOT-a plotting and regression program for radiogenic-isotope data. USGS Open-File Rept. 91-445. https://doi.org/10.3133/ofr91445

Ludwig, K. R., & Titterington, D. M. (1994). Calculation of isochrons, ages, and errors. *Geochimica et Cosmochimica Acta*, *58*(22), 5031–5042. https://doi.org/10.1016/0016-7037(94)90229-1

Vaks, A., Gutareva, O. S., Breitenbach, S. F. M., Avirmed, E., Mason, A. J., Thomas, A. L., et al. (2013). Speleothems reveal 500,000-year history of Siberian permafrost. *Science*, *340*(6129), 183–186. https://doi.org/10.1126/science.1228729